VOLUME 114, NUMBER 9
APRIL 22, 1992

JOURNAL
OF THE
AMERICAN
CHEMICAL
SOCIETY

Electron-Transfer Kinetics in Organized Thiol Monolayers with Attached Pentaammine(pyridine)ruthenium Redox Centers

Harry O. Finklea* and Dwight D. Hanshew

Contribution from the Department of Chemistry, West Virginia University, Morgantown, West Virginia 26506. *Received August 26, 1991. Revised Manuscript Received November 14, 1991*

Abstract: Thiols with pendant redox centers ($HS(CH_2)_nCONHCH_2pyRu(NH_3)_5^{2+}$, n = 10, 11, 15) adsorb from acetonitrile solutions onto gold electrodes to form electroactive monolayers. Mixed monolayers can be formed when the electroactive thiols are co-adsorbed with alkanethiols ($HS(CH_2)_nCH_3$, n = 11, 15) and ω-mercaptoalkanecarboxylic acids ($HS(CH_2)_nCOOH$, n = 10, 11, 15); the diluent thiol in each case is slightly shorter than the electroactive thiol. The $pyRu(NH_3)_5^{2+/3+}$ redox centers are stable in pH 4 aqueous Na_2SO_4 electrolyte and have a formal potential near 0.0 V vs SCE. At sufficiently slow scan rates, cyclic voltammograms of the electroactive monolayers are nearly ideal (peak splitting = 0 mV and peak half-width = 90–100 mV) for all combinations of electroactive thiol and diluent thiol and at all coverages of the electroactive thiols. The kinetics of electron transfer in the electroactive monolayers are examined by cyclic voltammetry and chronoamperometry. Evidence is given for the existence of a population of "fast" redox centers which can mediate charge transfer to the monolayer; however, rates of direct electron transfer between the electrode and the redox centers can be obtained. Experimental Tafel plots exhibit symmetric slopes in the cathodic and anodic branches, in contradiction to the prediction of through-space tunneling. The Tafel plots are fitted to Marcus theory to obtain the solvent reorganization parameter for the redox centers. The solvent reorganization parameter varies from 0.45 to 0.7 eV, with the parameter increasing with increasing chain length. Standard rate constants obtained from intercepts of the Tafel plots are primarily determined by the chain length and are independent of the terminal group in the diluent thiol. The standard rate constants tend to be larger for the anodic branch than for the cathodic branch, which implies slight differences in monolayer conformation for the two oxidation states of the redox centers. The standard rate constants for the mixed monolayers decay exponentially with increasing chain length. The slope of the ln $k°$ vs n plot is −1.06 (±0.04) per CH_2. Through-bond tunneling is proposed as the mechanism of electron transfer.

Introduction

Organized monolayers are attractive structures for controlling spacing with atomic resolution. Kuhn and co-workers[1] have demonstrated that both energy and electron transfer can be studied as a function of distance between two molecules if the molecules are imbedded in Langmuir–Blodgett monolayers. Tunneling junctions have been made with both Langmuir–Blodgett[2] and self-assembled monolayers[3] as spacers between two metals. An intriguing variation of the tunneling junction is an electrode coated with an organized monolayer. The monolayer serves as a precision spacer between the electrode and a redox couple, which may either be attached to the external surface of the monolayer or freely diffusing in the contacting electrolyte. As described below, the ability to control spacing with accuracy and high resolution permits the design of experiments which carefully test both the Marcus model of electron transfer and tunneling theory.

Because electron-transfer rate constants decrease rapidly with distance, the spacing experiment is restricted to a single organized layer of molecules on the electrode surface. We[4] and others[5-7]

(1) (a) Bucher, H.; Kuhn, H.; Mann, B.; Möbius, D.; von Szentpaly, L.; Tillman, P. *Photogr. Sci. Eng.* **1967**, *11*, 233–41. (b) Kuhn, H. *Pure Appl. Chem.* **1979**, *51*, 341–52.

(2) (a) Mann, B.; Kuhn, H. *J. Appl. Phys.* **1971**, *42*, 4398–405. (b) Polymeropoulos, E. E. *J. Appl. Phys.* **1977**, *48*, 2404–7. (c) Iizima, S.; Sugi, M. *Appl. Phys. Lett.* **1976**, *28*, 548–9. (d) Shigehara, K.; Hara, M.; Nakahama, H.; Miyata, S.; Murata, Y.; Yamada, A. *J. Am. Chem. Soc.* **1987**, *109*, 1237–8.

(3) Polymeropoulos, E. E.; Sagiv, J. *J. Chem. Phys.* **1978**, *69*, 1836–47.

(4) (a) Finklea, H. O.; Robinson, L. R.; Blackburn, A.; Richter, B.; Allara, D.; Bright, T. *Langmuir* **1986**, *2*, 239–44. (b) Finklea, H. O.; Avery, S.; Lynch, M.; Furtsch, T. *Langmuir* **1987**, *3*, 409–13. (c) Finklea, H. O.; Snider, D. A.; Fedyk, J. *Langmuir* **1990**, *6*, 371–6.

0002-7863/92/1514-3173$03.00/0

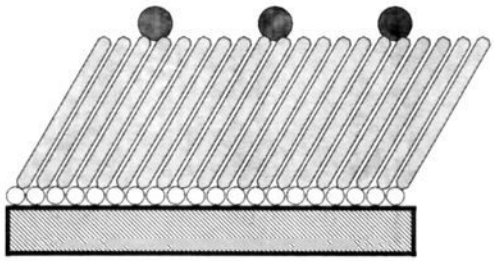

Figure 1. Mixed monolayer with electroactive and diluent thiols.

have explored the use of an organized monolayer, usually a self-assembled monolayer of alkanethiols on gold, as a blocking layer toward dissolved redox molecules. In most cases, electron transfer across the full width of the blocking monolayer is masked by faradaic reactions of molecules penetrating the monolayer, either at pinhole sites (exposed electrode surface) or at defect sites (collapsed or loosely packed monolayer structure). Miller and co-workers[7] have generated pinhole-free films of ω-hydroxyalkanethiols on gold and have evidence of tunneling across some as yet undefined thickness of the monolayer. Similarly, Lipkowski[8] and De Levie[9] have reported the formation of pinhole-free films of isoquinolines and thymines on mercury in the presence of a high concentration of these substances in the electrolyte.

The alternative approach is to attach the redox molecule to the external surface of the monolayer (Figure 1). In a well-oriented and close-packed monolayer, the redox center is held at a known and controllable distance from the electrode surface. Motion of the redox center toward the electrode is strongly inhibited by the steric interactions with nearest neighbors. As shown in Figure 1, a mixed monolayer composed of electroactive and nonelectroactive molecules allows a close-packed structure to form when the redox center radius does not match the average radius of the tether. The optimal length of the nonelectroactive diluent molecule is the same as the length of the tether.

There are several deviations from the ideal structure of Figure 1 which could compromise the measurements of electron-transfer kinetics: a disorganized monolayer which permits many kinks and twists of the tether, chain motion in a loosely packed monolayer, and crystallographic steps on the electrode surface. Therefore it is necessary to establish that a degree of order is present in the monolayer before rate constants are meaningful. As shown below, much information about the order of the monolayer can be gained from the electrochemical properties of the redox centers.

Self-assembled monolayers of alkanethiols on gold have been shown to be well-ordered and stable structures that survive electrochemical experiments.[4-7,10-26] Surface IR spectroscopy[5,10-13] indicates that the alkyl chains adopt a largely all-trans configuration with the chain axis tilted ca. 30° with respect to the surface normal. Electron[13b] and helium diffraction[11a,c] experiments reveal a close-packed hexagonal structure of both the thiols and the terminal methyl groups, with a nearest-neighbor spacing of 5 Å.

Alkanethiol monolayers with attached ferrocenes have already been reported.[11b,d,19] Mixed monolayers containing ω-ferrocenethiols well diluted with alkanethiols exhibit behavior consistent with a well-ordered structure.[11b] The cyclic voltammograms (CV's) of the monolayers under reversible conditions (slow scan rate) are ideal: peak splittings (ΔE_p) are 0 mV and peak half-widths (ΔE_{fwhm}) are 90 mV. However, the CV's become broad and ill-defined as the coverage of the ferrocene increases. In the first case, the formal potentials of all the redox centers are identical, which in turn implies that the environments around all of the redox centers are uniform. In the second case, a disordered structure is indicated in which some of the redox centers are buried in the monolayer and other centers are fully exposed to electrolyte. A disordered electroactive monolayer should exhibit an ensemble of formal potentials due to the varying dielectric constant around the redox centers.

A more stringent test for order can be obtained from measurements of the electron-transfer rate constants. Rate constants are most conveniently measured by chronoamperometry experiments. The electrode potential is stepped from an initial potential to a final potential to drive the oxidation or the reduction of the redox centers. At a given overpotential ($\eta = E - E^{\circ\prime}$), the current i follows a simple exponential decay:

$$i = k_{app} Q \exp(-k_{app} t) \quad (1)$$

where k_{app} is the apparent rate constant and Q is the charge

(5) (a) Porter, M. D.; Bright, T. B.; Allara, D.; Chidsey, C. E. D. *J. Am. Chem. Soc.* **1987**, *109*, 3559–68. (b) Chidsey, C. E. D.; Loiacono, D. N. *Langmuir* **1990**, *6*, 682–691.

(6) (a) Sabatani, E.; Rubinstein, I.; Maoz, R.; Sagiv, J. *J. Electroanal. Chem.* **1987**, *219*, 365–71. (b) Rubinstein, I.; Steinberg, S.; Tor, Y.; Shanzer, A.; Sagiv, J. *Nature* **1988**, *332*, 426–9. (c) Sabatani, E.; Rubinstein, I. *J. Phys. Chem.* **1987**, *91*, 6663–9. (d) Rubinstein, I.; Steinberg, S.; Tor, Y.; Shanzer, A.; Sagiv, J. *Nature* **1989**, *337*, 216–7. (e) Steinberg, S.; Tor, Y.; Sabatani, E.; Rubinstein, I. *J. Am. Chem. Soc.* **1991**, *113*, 5176–82.

(7) (a) Miller, C.; Cuendet, P.; Gratzel, M. *J. Phys. Chem.* **1991**, *95*, 877–86. (b) Miller, C.; Gratzel, M. *J. Phys. Chem.* **1991**, *95*, 5225–33.

(8) Lipkowski, J.; Buess-Herman, Cl.; Lambert, J. P.; Gierst, L. *J. Electroanal. Chem.* **1986**, *202*, 169–89.

(9) Srinivasan, R.; De Levie, R. *J. Electroanal. Chem.* **1986**, *201*, 145–52.

(10) (a) Nuzzo, R. G.; Allara, D. L. *J. Am. Chem. Soc.* **1983**, *105*, 4481–3. (b) Nuzzo, R. G.; Fusco, F. A.; Allara, D. L. *J. Am. Chem. Soc.* **1987**, *109*, 2358–68. (c) Nuzzo, R. G.; Dubois, L. H.; Allara, D. L. *J. Am. Chem. Soc.* **1990**, *112*, 558–69. (d) Dubois, L. H.; Zegarski, B. R.; Nuzzo, R. G. *J. Am. Chem. Soc.* **1990**, *112*, 570–9.

(11) (a) Chidsey, C. E. D.; Liu, G.-Y.; Rowntree, P.; Scoles, G. *J. Chem. Phys.* **1989**, *91*, 4421–3. (b) Chidsey, C. E. D.; Bertozzi, C. R.; Putvinski, T. M.; Mujsce, A. M. *J. Am. Chem. Soc.* **1990**, *112*, 4301–6. (c) Putvinski, T. M.; Schilling, M. L.; Katz, H. E.; Chidsey, C. E. D.; Mujsce, A. M.; Emerson, A. B. *Langmuir* **1990**, *6*, 1567–71. (d) Chidsey, C. E. D. *Science* **1991**, *251*, 919–22. (e) Chidsey, C. E. D.; Liu, G.; Scoles, G.; Wang, J. *Langmuir* **1990**, *6*, 1804–6.

(12) (a) Stole, S. M.; Porter, M. D. *Langmuir* **1990**, *6*, 1199–1202. (b) Walczak, M. M.; Chung, C.; Stole, S. M.; Widrig, C. A.; Porter, M. D. *J. Am. Chem. Soc.* **1991**, *113*, 2370–8. (c) Widrig, C. A.; Alves, C. A.; Porter, M. A. *J. Am. Chem. Soc.* **1991**, *113*, 2807–10.

(13) (a) Troughton, E. B.; Bain, C. D.; Whitesides, G. M.; Nuzzo, R. G.; Allara, D. L.; Porter, M. D. *Langmuir* **1988**, *4*, 365–85. (b) Strong, L.; Whitesides, G. M. *Langmuir* **1988**, *4*, 546–58. (c) Bain, C. D.; Whitesides, G. M. *J. Am. Chem. Soc.* **1988**, *110*, 3665–6. (d) Bain, C. D.; Whitesides, G. M. *J. Am. Chem. Soc.* **1988**, *110*, 5897–8. (e) Bain, C. D.; Whitesides, G. M. *J. Am. Chem. Soc.* **1988**, *110*, 6560–1. (f) Bain, C. D.; Whitesides, G. M. *Science* **1988**, *240*, 62–3. (g) Bain, C. D.; Troughton, E. B.; Tao, Y.-T.; Evall, J.; Whitesides, G. M.; Nuzzo, R. G. *J. Am. Chem. Soc.* **1989**, *111*, 321–35. (h) Bain, C. D.; Biebuyck, H. A.; Whitesides, G. M. *Langmuir* **1989**, *5*, 723–7. (i) Bain, C. D.; Whitesides, G. M. *J. Phys. Chem.* **1989**, *93*, 1670–3. (j) Bain, C. D.; Whitesides, G. M. *Langmuir* **1989**, *5*, 1370–8. (k) Bain, C. D.; Evall, J.; Whitesides, G. M. *J. Am. Chem. Soc.* **1989**, *111*, 7155–64. (l) Bain, C. D.; Whitesides, G. M. *J. Am. Chem. Soc.* **1989**, *111*, 7164–75. (m) Laibinis, P. E.; Hickman, J. J.; Wrighton, M. S.; Whitesides, G. M. *Science* **1989**, *245*, 845–7. (n) Whitesides, G. M.; Laibinis, P. E. *Langmuir* **1990**, *6*, 87–96.

(14) (a) Dubois, L. H.; Zegarski, B. R.; Nuzzo, R. G. *Proc. Natl. Acad. Sci. USA* **1987**, *84*, 4739–42. (b) Nuzzo, R. G.; Zegarski, B. R.; Dubois, L. H. *J. Am. Chem. Soc.* **1987**, *109*, 733–40. (c) Dubois, L. H.; Zegarski, B. R.; Nuzzo, R. G. *J. Am. Chem. Soc.* **1990**, *112*, 570–9.

(15) (a) De Long, H. C.; Buttry, D. A. *Langmuir* **1990**, *6*, 1319–22. (b) Nordyke, L. L.; Buttry, D. A. *Langmuir* **1991**, *7*, 380–8.

(16) (a) Ulman, A.; Evans, S. D.; Shnidman, Y.; Sharma, R.; Eilers, J. E.; Chang, J. C. *J. Am. Chem. Soc.* **1991**, *113*, 1499–1506. (b) Evans, S. D.; Sharma, R.; Ulman, A. *Langmuir* **1991**, *7*, 156–61.

(17) Lee, K. A. B. *Langmuir* **1990**, *6*, 709–12.

(18) Sobocinski, R. L.; Bryant, M. A.; Pemberton, J. E. *J. Am. Chem. Soc.* **1990**, *112*, 6177–83.

(19) (a) Creager, S. E.; Collard, D. M.; Fox, M. A. *Langmuir* **1990**, *6*, 1617–20. (b) Creager, S. E.; Rowe, G. K. *Anal. Chim. Acta* **1991**, *246*, 233–9. (c) Collard, D. M.; Fox, M. A. *Langmuir* **1991**, *7*, 1192–7.

(20) (a) Diem, T.; Czajka, B.; Weber, B.; Regen, S. L. *J. Am. Chem. Soc.* **1986**, *108*, 6094–5. (b) Fabianowski, W.; Coyle, L. C.; Weber, B. A.; Granata, R. D.; Castner, D. G.; Sadownik, A.; Regen, S. L. *Langmuir* **1989**, *5*, 35–41.

(21) Barner, B. J.; Corn, R. M. *Langmuir* **1990**, *6*, 1023–30.

(22) Arndt, Th.; Schupp, H.; Schrepp, W. *Thin Solid Films* **1989**, *178*, 319–26.

(23) Sandroff, C. J.; Garoff, S.; Leung, K. P. *Chem. Phys. Lett.* **1983**, *96*, 547.

(24) Obeng, Y. S.; Bard, A. J. *Langmuir* **1991**, *7*, 195–201.

(25) Samant, M. G.; Brown, C. A.; Gordon, J. G. *Langmuir* **1991**, *7*, 437–9.

(26) Thomas, R. C.; Sun, L.; Crooks, R. M.; Ricco, A. J. *Langmuir* **1991**, *7*, 620–2.

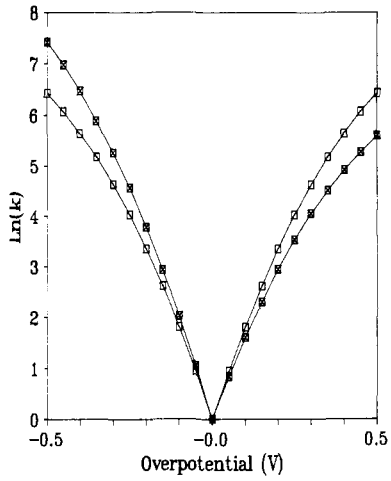

Figure 2. Simulated Tafel plots. The anodic rate constants are plotted for positive overpotential and the cathodic rate constants for negative overpotential; both are plotted relative to the standard rate constant. The open squares mark the Tafel plot for electron transfer without through-space tunneling, while the squares with crosses mark the Tafel plot which includes through-space tunneling with a barrier height of 2.4 eV and a barrier thickness of 20 Å (see the Appendix). The solvent reorganization energy is 0.6 eV in both plots.

associated with converting the redox centers from one oxidation state to the other. Consequently, a plot of ln i vs t (a CA plot) should be linear with a slope of $-k_{app}$, provided that all of the redox centers have the same apparent rate constant. Disorder in the monolayer should yield a spread of apparent rate constants. A simulation (see the supplementary material) of a chronoamperometry experiment for nonuniform rate constants shows that the CA plot has an apparent slope that decreases in magnitude as time increases; i.e., current flow at short times is dominated by the faster rate constants while current flow at longer times is dominated by the slower rate constants. When the deviation from linearity is sufficiently small to permit fitting the CA plot to a straight line, then the apparent charge obtained from the intercept at $t = 0$ (Q_{app} = −(intercept)/(slope)) is smaller than the actual charge.

Other causes besides disorder can yield a nonlinear CA plot. If the kinetics of charge transfer are limited by ion motion rather than by electron motion, then CA plots should show a negative deviation from linearity at short times (when the currents are highest). A diagnostic for this situation is a strong dependence of the apparent rate constants on electrolyte concentration and identity. A similar deviation is anticipated when the product of the current and the uncompensated resistance (iR drop) is large enough to significantly change the overpotential; the overpotential and hence k_{app} are no longer constant during the chronoamperometry experiment. Electron hopping from sites of rapid electron transfer ("fast" redox centers) to the remaining redox centers[27,28] may affect the linearity of CA plots if the electron hopping rate is comparable to the rate of direct electron transfer between the electrode and the redox centers. However, a linear CA plot does not eliminate electron hopping as a possible mechanism of charge transfer.

Assuming that apparent rate constants are obtainable from the (nearly) linear CA plots, then theories of long range electron transfer can be tested. The variation of the apparent rate constants with overpotential is normally displayed in a Tafel plot (ln k_{app} vs η). Chidsey[11d] showed that Tafel plots for the ferrocene-modified monolayers could be fit with a relatively simple treatment of the Marcus model. Only two parameters were required for a fit over a range of temperatures, the solvent reorganization parameter λ and a prefactor. Chidsey's treatment did not explicitly include tunneling. Schmickler and co-workers[29] considered the effects of tunneling through an energy barrier in conjunction with the Marcus model. A simple version of Schmickler's theoretical treatment is given in the Appendix, and the consequences of that theory are shown in a simulated Tafel plot (Figure 2). Marcus theory alone (tunneling not included) predicts that the Tafel plots will be curved, with the absolute slope decreasing as the absolute overpotential increases. At sufficiently large overpotential the rate constant becomes independent of overpotential (the equivalent of the Marcus "inverted" region in homogeneous electron transfer). If through-space tunneling is included, then the Tafel plot becomes asymmetrical. For any absolute overpotential, the magnitude of the slope is greater in the cathodic branch than in the anodic branch. In Figure 2, the transfer coefficient at $\eta = 0$ V is 0.50 for the Marcus theory alone, and 0.55 when through-space tunneling is included. The asymmetry arises from the change in the barrier height as the electrode potential changes; a more negative potential causes a decrease in the average barrier height, which in turn results in a greater rate of electron transfer. The degree of asymmetry is affected by the tunneling parameters, with asymmetry increasing as the barrier height E_B decreases and as the tunneling barrier thickness d increases.

The Tafel plots for the ω-ferrocenethiol monolayers[11d] did not exhibit the predicted asymmetry of through-space tunneling. Since some form of tunneling is required for electron transfer, the symmetrical Tafel plots imply the existence of a tunneling mechanism in which the coupling of the electron-transfer rate to distance is independent of electrode potential.

The rate of electron tunneling decreases exponentially with increasing distance:

$$k^\circ_{app} = k^\circ \exp(-\beta d) \qquad (2)$$

β is the tunneling parameter and k°_{app} is the apparent rate constant at zero overpotential. On the basis of studies of metal/monolayer/metal tunneling junctions,[2,3] we estimate a β of 1.3–1.8 Å^{-1} for through-space tunneling[30-32] (see the Appendix). Beratan and Hopfield[33] considered through-bond tunneling for an extended alkyl chain and calculated that β is 0.76 per methylene. Values of β that have been obtained in electrochemical experiments include 1.45 Å^{-1} for pentamminecobalt complexes adsorbed to a metal electrode via a pendant thiophene[34] and 1 Å^{-1} for mercury electrodes blocked by a pinhole-free layer of an isoquinoline derivative.[8] In both cases β was based on an assumed molecular orientation of the adsorbed layer.

We report here the electrochemical behavior of self-assembled monolayers containing thiols with the general formula HS-$(CH_2)_n$CONHCH$_2$pyRu$(NH_3)_5^{2+/3+}$ (n = 10, 11, 15; henceforth abbreviated HS–C$_n$–Ru). Monolayers containing only the electroactive thiol and monolayers containing both the electroactive and a diluent thiol are examined. The diluent thiol is either an alkanethiol (HS$(CH_2)_n$CH$_3$, n = 11 or 15; henceforth abbreviated HS–C$_n$–CH$_3$) or a (ω-mercaptoalkanecarboxylic acid (HS-$(CH_2)_n$COOH, n = 10, 11, 15; henceforth abbreviated HS–C$_n$–COOH). In each mixed monolayer, the length of the diluent thiol matches the alkyl chain length; i.e., n is the same for the

(27) (a) Daifuku, H.; Aoki, K.; Tokuda, K.; Matsuda, H. *J. Electroanal. Chem.* **1985**, *183*, 1–26. (b) Park, S. G.; Aoki, K.; Tokuda, K.; Matsuda, H. *J. Electroanal. Chem.* **1985**, *195*, 157–63.

(28) (a) Miller, C. J.; Majda, M. *J. Am. Chem. Soc.* **1986**, *108*, 3118–20. (b) Widrig, C. A.; Miller, C. J.; Majda, M. *J. Am. Chem. Soc.* **1988**, *110*, 2009–11. (c) Miller, C. J.; Widrig, C. A.; Charych, D. H.; Majda, M. *J. Phys. Chem.* **1988**, *92*, 1928–36. (d) Goss, C. A.; Miller, C. J.; Majda, M. *J. Phys. Chem.* **1988**, *92*, 1937–42.

(29) (a) Schmickler, W. *J. Electroanal. Chem.* **1977**, *82*, 65–80. (b) Schmickler, W.; Ulstrup, J. *Chem. Phys.* **1977**, *19*, 217–32. (c) Ulstrup, J. *Surf. Sci.* **1980**, *101*, 564–82. (d) Schmickler, W. *J. Electroanal. Chem.* **1977**, *83*, 387–91. (e) Schmickler, W. In *Passitivity of Metals and Semiconductors*; Froment, M., Ed.; Elsevier: Amsterdam, 1983; pp 23–33. (f) Schmickler, W. *J. Electroanal. Chem.* **1986**, *204*, 31–43.

(30) The true barrier height for the sandwich Al/Al_2O_3/monolayer/Al is calculated to be between 1.9 and 2.8 eV.[2,3] From the difference of work functions of aluminum and a metal electrode at 0 V vs SCE,[32] the true barrier height should lie between 2.4 and 3.3 eV for the Ru$(NH_3)_5$py redox center on the gold electrode. The true barrier height is reduced by image forces,[31] leading to estimates of 1.3–1.8 Å^{-1} for β.

(31) Simmons, J. G. *J. Appl. Phys.* **1963**, *34*, 1793–803.

(32) Frese, K. W., Jr. *J. Phys. Chem.* **1981**, *85*, 3911–6.

(33) Beratan, D. N.; Hopfield, J. J. *J. Am. Chem. Soc.* **1984**, *106*, 1584–94.

(34) Li, T. T.-T.; Weaver, M. J. *J. Am. Chem. Soc.* **1984**, *106*, 6107–8.

diluent and the electroactive thiol.

Experimental Section

Details of the thiol preparation and the conditions for monolayer formation will be reported elsewhere.[35] Synthesis of the electroactive thiols was based on the coupling of the pendant ammine of $Ru(NH_3)_5(4\text{-AMP})^{2+}$ (4-AMP = 4-(aminomethyl)pyridine) to the carboxylic acid or a ω-mercaptoalkanecarboxylic acid. Preparation of the ω-mercaptoalkanecarboxylic acids and the $Ru(NH_3)_5(4\text{-AMP})^{2+}$ followed standard literature procedures:[5b,13a,g,36]

$$Br(CH_2)_nCOOH + CH_3COS^- \rightarrow CH_3COS(CH_2)_nCOOH \rightarrow HS(CH_2)_nCOOH$$

$$Ru(NH_3)_5Cl^{2+} \rightarrow Ru(NH_3)_5(H_2O)^{2+} + HpyCH_2NH_3^{2+} \rightarrow Ru(NH_3)_5(pyCH_2NH_2)^{2+}$$

$$HS(CH_2)_nCOOH + Ru(NH_3)_5(pyCH_2NH_2)^{2+} \rightarrow HS(CH_2)_nCONHCH_2pyRu(NH_3)_5^{2+}$$

The final product was isolated as the PF_6^- salt. At all stages, the redox center was kept in the reduced oxidation state (Ru(II)) to avoid oxidation of the thiol. Proof of the structure of the final product was based on NMR and IR spectroscopy, and cyclic voltammetry in aqueous and acetonitrile electrolytes.

The $pyRu(NH_3)_5^{2+}$ species were handled under red light and stored in the dark to avoid photochemical loss of the pyridine.[36] The exclusion of UV and blue light applied in particular to the deposition of the monolayers and the subsequent characterization of the coated electrodes.

Monolayers were formed by self-assembly on gold mirror electrodes. The gold mirror electrodes (1 × 3 cm), purchased from Evaporated Metal Films, Inc. (Ithaca, NY), consisted of float glass covered first with 50 Å of Ti followed by 1000 Å of gold. The gold mirrors were cleaned by sonication in chloroform followed by immersion for 30 s in "piranha" solution (3:1 mixture of concentrated H_2SO_4 and 30% H_2O_2 heated to ca. 100 °C) (*CAUTION*: *"piranha" solution reacts violently with organic material!*). After rinsing with deionized water (Corning MegaPure system) and drying with a hot-air gun, the mirrors were immersed in 20 mL of the deposition solution. Upon removal from the deposition solution, the electrodes were rinsed with acetonitrile and then water. The procedure that produced the most ideally behaved monolayers consisted of repeated immersions of the electrode in the deposition solution followed by cyclic voltammetry in aqueous electrolyte (see below).

Deposition solutions typically were 10^{-4}–10^{-3} M total concentration of the thiols in acetonitrile. Deposition solutions containing both the electroactive thiol and the diluent thiol were prepared by mixing appropriate volumes of solutions containing only the electroactive thiol or the diluent thiol. All solutions containing the electroactive thiols were passed through a 0.4-μm filter prior to use as a deposition solution. The coverage of the redox centers could be varied by adjusting the mole ratio of the electroactive thiol to the diluent thiol in the deposition solution.[35]

Electrochemical experiments were performed in a two-compartment cell at room temperature (22 °C). The working electrode (gold mirror with an immersed area of 1 cm^2) was centered with respect to the cylindrical coil of the gold counter electrode. A wide-bore (2-mm) Luggin capillary connected the reference and working compartments; the capillary contained an unconnected gold wire to lower its impedance.[37] The uncompensated resistance of the cell (measured by ac voltammetry) was 14 Ω in 0.2 M Na_2SO_4 and 5 Ω in 1 M Na_2SO_4, both at pH 4. The pH was a compromise between stability of the attached redox centers (which rapidly disappear in pH 8 electrolyte) and the range of negative overpotential available before the onset of electrolyte reduction. Interfacial capacitances for the monolayer-coated electrodes varied between 2 and 5 $\mu F/cm^2$; consequently, charging currents were negligible after ca. 0.3 ms. Electrolytes were sparged with argon prior to voltammetry and blanketed with argon during voltammetry. Cyclic voltammograms were recorded using a Bioanalytical Systems CV-27 potentiostat; because of the 1-ms time constant of the current follower in the CV-27, some distortion of the CV's appeared at the fastest scan rates (10 V/s). Chronoamperometry experiments were performed using a Princeton Applied Research Model 173 potentiostat. Current was converted to voltage with a resistor in series with the counter electrode and connected to an instrumentation amplifier (gain of 3). The time constant of the 173 potentiostat and current follower was ca. 10^{-5} s. In the chronoamperometry experiment, a square wave of amplitude 2η was combined with a dc potential equal to the formal potential of the attached redox centers (Figure 3). Current was collected for both the positive and negative potential steps and analyzed for k_{app} at the corresponding overpotentials. The CV and the CA experiments were interfaced to a Zenith XT computer with a Metrabyte DASH-16 interface board. ASYSTANT+ software (MacMillan) was used to acquire and analyze data.

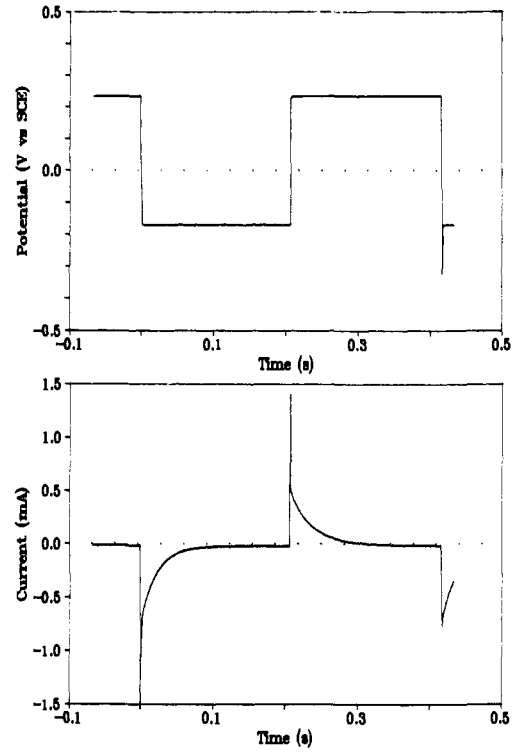

Figure 3. Potential–time and current–time transients for the chronoamperometry experiment. The potential step is symmetrical about the formal potential so that both the anodic and the cathodic rate constants could be determined in one experiment. The time of each potential step is long enough to allow the current to decay to base line levels. In this figure, a 100% $HS–C_{15}–Ru$ monolayer with $E^{\circ\prime} = -0.020$ V vs SCE is subjected to overpotentials of ±0.20 V in 1 M Na_2SO_4.

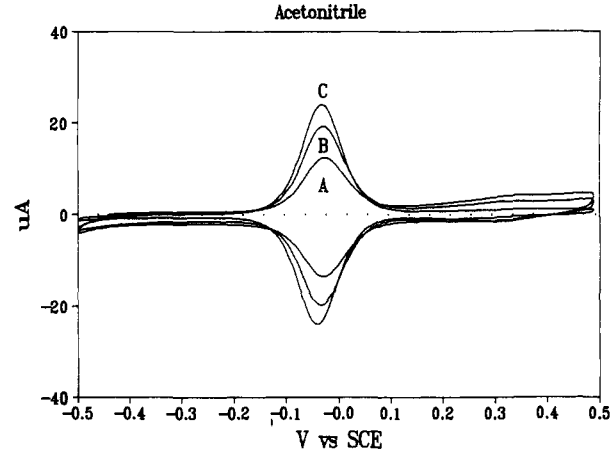

Figure 4. Reversible CV's of 100% $HS–C_n–Ru$ monolayers. All CV's are acquired in 0.2 M Na_2SO_4 at 0.1 V/s with an immersed electrode area of 1.0 cm^2. Each electrode has been subjected to five successive immersions in the acetonitrile deposition solution (3-h cumulative deposition time) alternated with CV's in aqueous electrolyte. A. $HS–C_{10}–Ru$. B. $HS–C_{11}–Ru$. C. $HS–C_{15}–Ru$.

Results and Discussion

Reversible Cyclic Voltammetry. Typical cyclic voltammograms for 100% $HS–C_n–Ru$ monolayers are shown in Figure 4. At sufficiently slow scan rates (typically 0.1 V/s or slower), the CV's of both 100% $HS–C_n–Ru$ monolayers and mixed monolayers with either diluent thiol all display a common set of characteristics:[35]

(35) Finklea, H. O.; Hanshew, D. D. Manuscript in preparation.
(36) (a) Ford, P.; Rudd, D. F. E.; Gaunder, R.; Taube, H. *J. Am. Chem. Soc.* **1968**, *90*, 1187–94. (b) Kuehn, C. G.; Taube, H. *J. Am. Chem. Soc.* **1976**, *98*, 689–702.
(37) Fletcher, S.; Horne, M. D. *J. Electroanal. Chem.* **1991**, *297*, 297–9.

(a) The formal potential of the redox centers (between 0.00 and −0.10 V vs SCE) is close to the formal potential of a solution analogue, $CH_3CONHCH_2pyRu(NH_3)_5^{2+/3+}$ (+0.04 V vs SCE). The formal potential of the redox centers shifts toward the formal potential of the solution analogue as the coverage of the redox centers decreases.

(b) On each CV, the integrated charges of the anodic peak and the cathodic peak are identical within experimental error and are independent of the scan rate.

(c) The peak splitting (ΔE_p) is 0 mV within experimental uncertainty (±4 mV).

(d) The peak half-widths (ΔE_{fwhm}) are 90–100 mV.

From the above characteristics we conclude that the redox centers are fully solvated by the aqueous electrolyte. The formal potentials are identical for all of the redox centers, which implies that the local environment around each redox center is remarkably uniform. All of the redox centers are rapidly exchanging electrons with the electrode on the time scale of the experiment. The reversible CV data point to an ordered structure with all of the redox centers outside of the hydrocarbon portion of the monolayer.

It is noteworthy that the virtually ideal voltammetry of the redox centers is independent of the length of the alkyl chain, the ratio of the electroactive thiols to the diluent thiols in the monolayer, and the nature of the functional group at the terminus of the diluent thiol. The ferrocene monolayers reported by Chidsey[11b] only exhibit ideal CV's when the coverage of the ferrocene redox centers is relatively low. We attribute the remarkable behavior of the $HS-C_n-Ru$ monolayers to the hydrophilicity of the $pyRu(NH_3)_5^{2+/3+}$ redox centers. Submersion of the redox centers into the hydrocarbon domain is not favored even when the monolayer is not close-packed.

The maximum coverages observed for the 100% $HS-C_n-Ru$ monolayers range between 10 and 20 $\mu C/cm^2$ of geometric area. Since the surface roughness factor of the gold mirror electrodes is approximately 1.2,[38-40] the average separation between thiols is 10–14 Å. This average separation exceeds considerably the 5-Å spacing between chains in a close-packed alkanethiol monolayer. Electron hopping from fast redox centers to more remote centers may be a major mode of charge transport during a voltammetry experiment, partly because of the proximity between redox centers and partly because of the free volume which allows chain motion. Electron-transfer rates are significantly faster for the 100% $HS-C_{15}-Ru$ monolayers than for mixed monolayers containing $HS-C_{15}-Ru$ (see below). Coverages in the mixed monolayers range between 3 and 10 $\mu C/cm^2$, with an average value of 6 $\mu C/cm^2$ (average spacing, 19 Å). Within the uncertainties in the kinetic measurements (including reproducibility for monolayers produced from the same deposition solution), we observe no dependence of the electron-transfer rates on coverage in the mixed monolayers.

In the reversible CV's, the major difference between mixed monolayers with either $HS-C_n-CH_3$ or $HS-C_n-COOH$ as the diluent is the coverage of the redox centers.[35] For a given mole ratio of electroactive thiol to diluent thiol in the deposition solution, alkanethiols yield considerably lower coverages of the redox centers than do ω-mercapto carboxylic acids. Both diluent thiols compete effectively with the electroactive thiol for adsorption sites on the gold.

Electron-Transfer Kinetics from Cyclic Voltammetry. CV's of all of the monolayers exhibit kinetic peak splitting when the scan rate is sufficiently large (Figure 5). The peak splitting can be translated into the apparent standard rate constant ($k°_{app}$) provided that the transfer coefficient is known.[41] We find that peak splitting provides a rapid and qualitative tool for following the effects of various treatments of the monolayer on electron-transfer kinetics. Repeated immersions of the electrode in the deposition solution alternated with CV's in aqueous electrolyte lead to larger peak splittings (lower standard rate constant). Immersion of the monolayer-coated electrode in an acetonitrile solution containing only the diluent thiol usually results in an increase in peak splitting only when the electroactive thiol is $HS-C_{15}-Ru$; no change is observed for the shorter chain electroactive thiols. Since coverage of the $pyRu(NH_3)_5$ redox centers does not change significantly, we hypothesize that adsorption of additional diluent thiol decreases chain motion by intercalation of the diluent thiol into the existing monolayer.

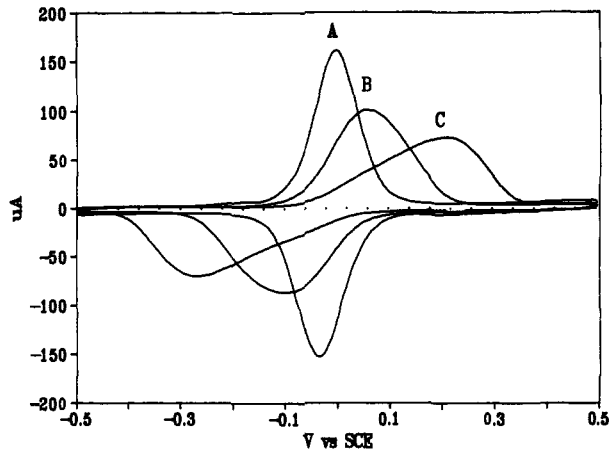

Figure 5. Irreversible CV's of a 100% $HS-C_{15}-Ru$ monolayer. The CV's are acquired in 0.2 M Na_2SO_4 with an immersed area of 1.0 cm^2. Curves A–C are for scan rates of 0.10, 1.0, and 5.0 V/s. The currents have been normalized to a scan rate of 1.0 V/s.

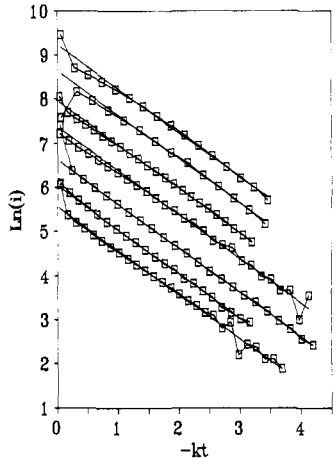

Figure 6. Chronoamperometry plots for a 100% $HS-C_{15}-Ru$ monolayer in 1.0 M Na_2SO_4. Both data (open squares) and the linear regression line are shown. The abscissa is the product of the slope of the linear regression line (k) and time (t). The approximate overpotentials are (top to bottom) 0.40, 0.35, 0.30, 0.25, 0.20, 0.16, and 0.12 V. CA plots for the corresponding negative overpotentials are similar.

Quantitative conversion of peak splitting to $k°_{app}$ is less certain due to several factors. Laviron's theory and tables[41] assume that the transfer coefficient is independent of potential; the Tafel plots show that the transfer coefficient changes markedly with potential. Similarly, the theory assumes that the rate constants are uniform for all redox centers. We observe a considerable broadening of the peak half-widths in CV's with small peak splitting (<50 mV) and occasionally a shoulder on the low overpotential side of a CV with a large peak splitting (>200 mV) (see Figure 5, curve C). The shoulder with smaller ΔE_p and the extra broad CV's both indicate that the rate constant is not uniform, and that there exists a population of redox centers with a somewhat faster standard rate constant. Despite these adverse factors, $k°_{app}$ values from ΔE_p values assuming a transfer coefficient of 0.5 are reported in Table I. Agreement of the CV $k°_{app}$ values with $k°_{app}$ values from Tafel plots is in most cases within a factor of 2.

(38) The true surface area of a gold electrode can be obtained from anodic stripping of adsorbed iodide[39] and from underpotential deposition of silver and copper.[40]

(39) Rodriguez, J. F.; Mebrahtu, T.; Soriaga, M. P. *J. Electroanal. Chem.* **1987**, *233*, 283–9.

(40) Deakin, M. R.; Melroy, O. *J. Electroanal. Chem.* **1988**, *239*, 321–31.

(41) Laviron, E. *J. Electroanal. Chem.* **1979**, *101*, 19–28.

Table I. Standard Rate Constants for Electron Transfer from Cyclic Voltammetry and Tafel Plots[a]

monolayer composn	Q_t, μC	concn, M	XC	ν, V/s	ΔE_p, mV	$k°_{app}$, s^{-1} CV	anodic	cathodic	CA
1. $HS-C_{15}-Ru$	12.9	0.2	N	0.1	26	5.4	1.3	0.90	A
				1.0	145	5.4			
				10.0	622				
2. $HS-C_{15}-Ru$	16.8	0.2	N	0.1	32	4.3	1.6	1.1	B
				1.0	152	4.9			
				5.0	474	0.96			
2. $HS-C_{15}-Ru$	18.1	1.0	N	0.1	25	5.6	2.0	1.0	C
				1.0	125	6.9			
				5.0	427	1.5			
3. $HS-C_{15}-Ru$	10.8	1.0	N	0.1	13		1.2	0.90	D
4. $HS-C_{15}-Ru/HS-C_{15}-COOH$	2.8	0.2	N	0.1	155	0.48	0.45	0.41	E
				1.0	412	0.35			
4. $HS-C_{15}-Ru/HS-C_{15}-COOH$	2.8	1.0	N	0.1	127	0.67	0.55	0.33	E
				1.0	400	0.40			
5. $HS-C_{15}-Ru/HS-C_{15}-COOH$	6.4	1.0	N	0.1	125	0.69	0.45	0.45	F
6. $HS-C_{15}-Ru/HS-C_{15}-COOH$	10.0	1.0	N	0.1	41	3.2	0.61	0.37	F
				1.0	334	0.76			
7. $HS-C_{11}-Ru/HS-C_{11}-COOH$	6.7	1.0	N	1.0	28	50	40	37	G
				10.0	163	43			
7. $HS-C_{11}-Ru/HS-C_{11}-COOH$	6.9	1.0	Y	1.0	28	50	45	40	G
				10.0	172	39			
8. $HS-C_{10}-Ru/HS-C_{10}-COOH$	6.6	1.0	N	1.0	16		90	81	G
				10.0	103	93			
8. $HS-C_{10}-Ru/HS-C_{10}-COOH$	6.4	1.0	Y	1.0	16		110	90	G
				10.0	102	94			
9. $HS-C_{15}-Ru/HS-C_{15}-CH_3$	3.2	0.2	N	0.1	86	1.2	0.61	0.45	E
				1.0	422	0.32			
				10.0	759				
10. $HS-C_{15}-Ru/HS-C_{15}-CH_3$	3.3	1.0	N	0.1	22	6.5	0.67	0.45	D
11. $HS-C_{11}-Ru/HS-C_{11}-CH_3$	4.6	1.0	N	1.0	41	32	30	25	H
				10.0	201	29			
11. $HS-C_{11}-Ru/HS-C_{11}-CH_3$	3.5	1.0	Y	1.0	47	27	30	25	H
				10.0	208	27			

[a] The columns contain (1) the composition of the monolayer, (2) the integrated charge per cm^2 from CV's, (3) the concentration of the Na_2SO_4 electrolyte, (4) indication, of whether the monolayer has been "exchanged" with the diluent thiol, (5) the CV scan rate, (6) the CV peak splitting, (7) the CV standard rate constant, (8) the standard rate constant from the anodic branch of the Tafel plot, (9) the standard rate constant from the cathodic branch of the Tafel plot, and (10) a code describing the behavior of the CA plots. Rows with the same number refer to the same monolayer. The code descriptions are: (A) linear at all overpotentials and times; (B) at short times, positive deviation from the straight line at small $|\eta|$, negative deviation at large $|\eta|$; (C) at short times, positive deviation at small $|\eta|$; (D) at short times, positive deviation at all $|\eta|$; (E) at short times, positive deviation from the straight line at large $|\eta|$; (F) linear for negative η, positive deviation for positive η at short time; (G) at short times, negative deviation at large $|\eta|$, positive deviation at long times; (H) considerable deviation from a straight line at all times and all $|\eta|$.

Chronoamperometry. Chronoamperometry of electrodes coated with the pure electroactive thiol monolayers (no diluent thiol) in 1 M Na_2SO_4 yield nearly linear CA plots (Figure 6). The CA plots have kt (where k is the slope of the linear regression line) as the abscissa so that current transients at different potentials can be compared. Q values obtained from the slope and intercept of the linear regression lines (see eq 1) match Q values obtained by CV within 15%; this condition confirms that all of the redox centers are being observed during the current–time transient. Deviations of the CA plots from linearity occur most frequently at low overpotentials and short times. The deviations are consistent with a small population of fast redox centers in the monolayer. The fast redox centers do not control the electron-transfer kinetics to the all of the redox centers; otherwise the CA plots would be linear.

At short times and for large overpotentials in 0.2 M Na_2SO_4, another type of deviation appears in the CA plots (Figure 7). The experimental points fall below the linear regression line (which is determined at the point of steepest slope). The deviation is consistent with iR drop effects. With peak currents exceeding 1 mA and an uncompensated resistance of ca. 14 Ω, the iR drop is greater than 10 mV, which decreases the overpotential sufficiently to affect the rate of electron transfer. The deviation becomes negligible when the uncompensated resistance is lowered by raising the electrolyte concentration.

In general, CA plots of the mixed monolayers follow the pattern observed for the pure $HS-C_{15}-Ru$ monolayers (see the supplementary material). The plots are linear over a range of kt of 1–3. Typically, standard deviations of the slopes are less than 1% of the slopes. The extrapolated intercepts yield charges which either

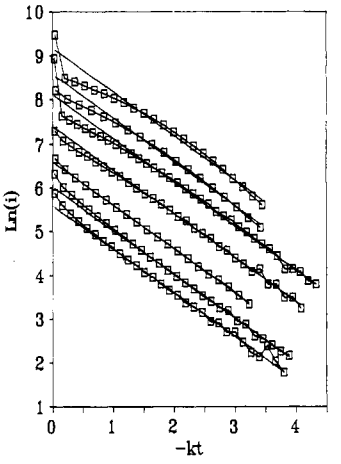

Figure 7. Chronoamperometry plots for the 100% $HS-C_{15}-Ru$ monolayer of Figure 6 in 0.2 M Na_2SO_4. The overpotentials are the same as in Figure 6.

agree well with the actual charge (from the CV's) or are smaller than the actual charge by 20–50%. In the latter cases, the initial currents are significantly above the linear repression line. As noted above, the discrepancy in the extrapolated charge and the deviation in the initial currents from single exponential decay are attributed to a population of fast redox centers which do not communicate readily with the remaining redox centers. The Tafel plots of this study are based on the slower rate constants. The general form

Table II. Apparent Transfer Coefficients from Tafel Plots[a]

monolayer composn	electrolyte concn, M	α anodic	α cathodic
1. $HS-C_{15}-Ru$	0.2	0.33	0.31
2. $HS-C_{15}-Ru$	0.2	0.33	0.31
2. $HS-C_{15}-Ru$	1.0	0.35	0.34
3. $HS-C_{15}-Ru$	1.0	0.32	0.28
average (SD)		0.33 (0.01)	0.31 (0.02)
4. $HS-C_{15}-Ru/HS-C_{15}-COOH$	0.2	0.36	0.37
4. $HS-C_{15}-Ru/HS-C_{15}-COOH$	1.0	0.31	0.30
5. $HS-C_{15}-Ru/HS-C_{15}-COOH$	1.0	0.37	0.35
6. $HS-C_{15}-Ru/HS-C_{15}-COOH$	1.0	0.34	0.34
average (SD)		0.35 (0.03)	0.34 (0.03)
7. $HS-C_{11}-Ru/HS-C_{11}-COOH$	1.0	0.26	0.27
7. $HS-C_{11}-Ru/HS-C_{11}-COOH$	1.0	0.28	0.26
average		0.27	0.27
8. $HS-C_{10}-Ru/HS-C_{10}-COOH$	1.0	0.28	0.26
8. $HS-C_{10}-Ru/HS-C_{10}-COOH$	1.0	0.32	0.29
average		0.30	0.28
9. $HS-C_{15}-Ru/HS-C_{15}-CH_3$	0.2	0.33	0.31
10. $HS-C_{15}-Ru/HS-C_{15}-CH_3$	1.0	0.29	0.28
average		0.31	0.30
11. $HS-C_{11}-Ru/HS-C_{11}-CH_3$	1.0	0.29	0.27
11. $HS-C_{11}-Ru/HS-C_{11}-CH_3$	1.0	0.27	0.25
average		0.28	0.26

[a] The transfer coefficients (α's) are the product of RT/F (0.0257) and the absolute slope of the Tafel plot from $|\eta| = 0.2$–0.3 V. The row numbers of this table and Table I correspond to the same monolayers. SD = standard deviation.

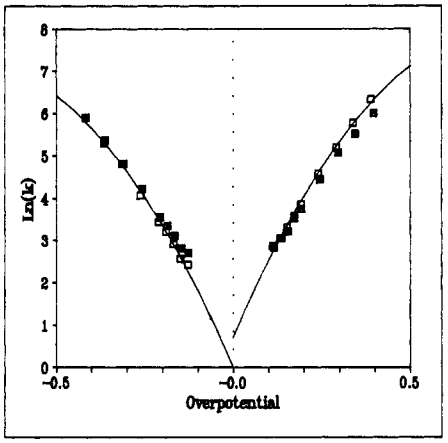

Figure 8. Tafel plots of a 100% $HS-C_{15}-Ru$ monolayer in 1.0 M Na_2SO_4 (open squares) and 0.2 M Na_2SO_4 (squares with X's). Theoretical Tafel curves are shown for $\lambda = 0.6$ eV (no through-space tunneling). The curves are independently fitted to the anodic and cathodic branches of the data acquired in 1.0 M Na_2SO_4.

of each CA plot is noted in Table I.

Tafel plots of a 100% $HS-C_{15}-Ru$ monolayer are shown in Figure 8. The Tafel plot contains the rate constants obtained from the CA plots of Figures 6 and 7. The two sets of points correspond to two concentrations of electrolyte, 0.2 and 1.0 M Na_2SO_4. Overlap of the two plots is within experimental uncertainty, as indicated by the reproducibility of the Tafel plot of a single monolayer in one electrolyte. Because double layer effects on electron-transfer kinetics are usually evident when the electrolyte concentration is varied,[42] we infer that double layer effects (e.g., variations of the potential at the boundary between the monolayer and the electrolyte with electrode potential) are negligible in this system. The plot exhibits curvature of the type predicted by the Marcus model; the absolute slope of the Tafel plot decreases with increasing absolute overpotential.

Table III. Theoretical Transfer Coefficients at $|\eta| = 0.25$ V[a]

λ, eV	α	λ, eV	α	λ, eV	α
0.40	0.263	0.50	0.300	0.70	0.344
0.45	0.283	0.60	0.328	0.80	0.365

[a] The transfer coefficients are based on the Marcus model (see the Appendix) with $\alpha = 0.5$ at $\eta = 0$.

Table IV. Solvent Reorganization Parameters as a Function of Monolayer Composition

monolayer composn	average α	λ, eV
$HS-C_{15}-Ru$	0.32	0.6
$HS-C_{15}-Ru/HS-C_{15}-COOH$	0.35	0.7
$HS-C_{11}-Ru/HS-C_{11}-COOH$	0.27	0.45
$HS-C_{10}-Ru/HS-C_{10}-COOH$	0.28	0.45
$HS-C_{15}-Ru/HS-C_{15}-CH_3$	0.30	0.5
$HS-C_{11}-Ru/HS-C_{11}-CH_3$	0.27	0.45

Our analyses of all of the Tafel plots (see the supplementary material) are based on the following observations. The steepest slopes of both the anodic and the cathodic branches are not at the lowest overpotentials, but in the absolute overpotential range of 0.2–0.3 V. Table II lists the apparent transfer coefficients at $\eta = +0.25$ and -0.25 V for monolayers grouped by composition. One immediate fact is made apparent by comparing the anodic and the cathodic transfer coefficient for each monolayer. *There is no significant difference in the magnitude of the anodic and cathodic transfer coefficients.* We conclude that (a) the transfer coefficient at $\eta = 0$ is 0.5 for the $pyRu(NH_3)_5$ redox center, (b) the solvent reorganization parameter is the same for the oxidized and reduced forms of the redox center, and (c) the through-space tunneling model is incorrect. It is conceivable that an inequality of the transfer coefficients for the redox center is offset by the effects of tunneling, but that hypothesis is made untenable by the presence of symmetrical slopes in Tafel plots for all three chain lengths. Consequently, the mechanism of long range electron transfer in this system must have a tunneling factor which is independent of the electrode potential or which changes symmetrically with absolute overpotential.

(42) Delahay, P. *Double Layer and Electrode Kinetics*; Interscience: New York, 1966.

Table II also reveals significant differences in the apparent transfer coefficients as the composition of the monolayer is varied. In order to extract k°_{app}, we vary the solvent reorganization energy λ to fit the average transfer coefficient of each type of monolayer. λ is obtained from Table III, which lists theoretical transfer coefficients from Tafel plots calculated as in Figure 2. Table IV contains the average transfer coefficients and the λ values used in the analyses of the Tafel plots. The uncertainty in the λ values used to fit the Tafel plots is estimated to be ±0.1 eV. We note two interesting trends: the λ values decrease as the alkyl chain lengths of the monolayers decrease, and the λ values of the HS–C_{15}–Ru monolayers change significantly as a function of the monolayer composition.

The fitted λ values are considerably smaller than predicted by the Marcus model. In the Marcus model, λ is the sum of an inner sphere and an outer sphere component. The inner sphere component, which is largely determined by the composition of the redox center, is estimated to be 0.17 eV for $pyRu(NH_3)_5^{2+/3+}$.[43] The outer sphere component is given by the expression[44]

$$\lambda_{os} = (e^2N/2)((1/a) - (1/(2d)))((1/\epsilon_{op}) - (1/\epsilon_s)) \quad (3)$$

N is Avogadro's number, a is the radius of the redox center, d is the distance of the redox center from the electrode, and ϵ_{op} and ϵ_s are the optical and static dielectric constants of the medium around the redox center. The $Ru(NH_3)_5py$ redox center is not spherical; CPK models[43] indicate that the radius varies between 3.3 and 5.1 Å. With a mean value of 3.8 Å for a, approximate distances of 17–23 Å for all of the monolayers (a 30° tilt in the main axis of the alkyl chain is assumed), and the dielectric constants of pure water, eq 3 yields a value of 0.92–0.95 eV for λ_{os}; hence, λ is 1.1 eV, roughly twice as large as the observed values. Chidsey[11d] observed a smaller discrepancy between the fitted λ (0.85 eV) and the λ_{os} predicted by eq 3 (0.94 eV).

Several explanations for the substantial disagreement between the fitted and theoretical λ's are possible. First, the effective radius of the redox center may be larger because it is tethered through the pyridine; i.e., the long axis of the redox center is perpendicular to the electrode. If d is 5.1 Å, then eq 3 yields a value of 0.7 eV for λ_{os}. Second, the local static dielectric constant may be substantially smaller for a redox center near a hydrocarbon layer. A smaller ϵ_s leads to a smaller value of λ_{os}. A decrease in ϵ_s would also account for the decrease in λ between the HS–C_{15}–COOH mixed monolayers and the HS–C_{15}–CH_3 mixed monolayers. Third, other theoretical equations for estimating λ may be more appropriate.[45]

Examination of the Tafel plots (Figure 8 and supplementary material) reveal two other observations. First, the data points at low overpotentials often deviate above the theoretical Tafel lines (which are fitted at $|\eta| = 0.25$ V). The deviation is most evident when the CA plots indicate the presence of a significant population of fast redox centers. We propose that electron hopping from the fast redox centers to the remaining centers augments the apparent rate of electron transfer at low overpotentials. As the absolute overpotential increases, the rate of direct electron transfer between the electrode and the redox center becomes faster than the rate of electron hopping from the fast redox centers. Hence, the rate constants at large absolute overpotential are believed to be valid for direct rather than mediated electron transfer.

Second, the intercepts of the theoretical lines frequently differ for the anodic and cathodic branches of the Tafel plots. In every case where a significant difference in the intercepts exists, k°_{app} for the anodic branch is larger (by as much as a factor of 2) than k°_{app} for the cathodic branch. We propose that the difference arises from a slight change in the monolayer conformation with either the oxidation state of the redox center or the electrode potential. Without knowing the rate at which the monolayer

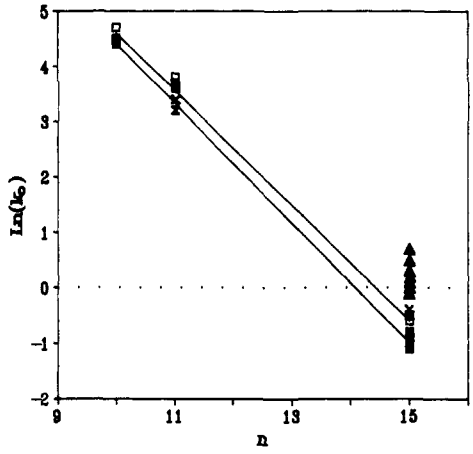

Figure 9. Distance dependence of the standard rate constants. The abscissa is the number of CH_2's in the alkyl chain. Data points are shown for 100% HS–C_{15}–Ru monolayers (filled triangles), HS–C_n–Ru/HS–C_n–COOH monolayers (open squares, anodic k°; squares with X's, cathodic k°) and HS–C_n–Ru/HS–C_n–CH_3 monolayers (X's, anodic k°; hour glasses, cathodic k°). Separate linear regression lines appear for the anodic (upper line) and cathodic (lower line) k°'s.

conformation adjusts to the charge of the redox center or to the potential of the electrode, it is difficult to assign the faster rates of the anodic branch to the initial conformation or to the final conformation during the CA experiment. Molecular dynamics simulations of monolayers[46] suggest that conformation changes may be quite fast (on the order of nanoseconds) compared to the CA experiments (milliseconds to seconds). Given that hypothesis, the measured rate constants reflect both the rate of electron transfer and the changing conformation of the monolayer. However, the difference between anodic and cathodic standard rate constants is small enough that the distance dependence can be examined.

When ln k°_{app} values are plotted vs n for all of the monolayers (Figure 9), one fact becomes immediately evident: *the primary determinate of the standard rate constant is the chain length.* In particular, all of the mixed monolayers yield the same standard rate constants within a factor of 2. Neither the coverage of the redox centers in the mixed monolayers nor the identity of the diluent thiol appear to affect the standard rate constant. It is noteworthy that the insertion of a single CH_2 into the alkyl chain connecting the redox center to the electrode has a marked effect on the standard rate constant. Only the 100% HS–C_{15}–Ru monolayers exhibit a significantly faster standard rate constant. The faster rate may be the consequence of the smaller spacing between redox centers (which enhances electron hopping from fast redox centers), greater motion because of looser packing of the alkyl chains, or differences in monolayer conformation for the 100% HS–C_{15}–Ru monolayers.

Given the evidence for direct rather than mediated electron transfer, the standard rate constants can be examined in terms of the fundamental distance relation of electron tunneling, eq 2. Linear regression lines are shown in Figure 9 for both the anodic and the cathodic standard rate constants of the mixed monolayers. The values of the tunneling parameter β are (anodic) 1.04 ± 0.02 per CH_2 and (cathodic) 1.08 ± 0.02 per CH_2. If the electroactive monolayers are assumed to adopt a configuration inferred for alkanethiol monolayers (all-trans configuration, 30° tilt of the chain axes, 1.27 Å per CH_2), then the corresponding values of β are 0.95 and 0.98 $Å^{-1}$. These numbers are close to the theoretical β (0.76 per CH_2) for through-bond tunneling[33] and substantially smaller than the estimated β (1.3–1.8 $Å^{-1}$) for classical electron tunneling through an energy barrier (see the Appendix). Since symmetrical slopes in the Tafel plots also contradict electron tunneling through space, we hypothesize that *the mechanism of electron transfer is through-bond tunneling.* The agreement

(43) Brown, G. M.; Sutin, N. *J. Am. Chem. Soc.* **1979**, *101*, 883–94.
(44) (a) Marcus, R. A. *J. Phys. Chem.* **1963**, *67*, 853–7. (b) Marcus, R. A. *J. Chem. Phys.* **1965**, *43*, 679–701.
(45) Baranski, A. S.; Winkler, K.; Fawcett, W. R. *J. Electroanal. Chem.* **1991**, *313*, 367–75.
(46) Hautman, J.; Klein, M. L. *J. Chem. Phys.* **1989**, *91*, 4994–5001.

between the theoretical β[33] and β for this system is reasonable given the uncertainties in the actual alkyl chain conformation and the presence of the amide bond in the chain.

Further experimentation with respect to chain length and functional groups between the thiol and the redox center would be interesting. However, the HS–C_{10}–Ru monolayers are the practical lower limit for chain length. In these monolayers, rate constants above 1000 s^{-1} are reached at rather low absolute overpotentials. Rate constants above 5000 s^{-1} are subject to considerable error because of the difficulty of separating the charging current transient from the quasi-exponential decay of electron transfer. Both iR drop and the rate of ion motion may also hinder the measurement of the electron-transfer rate constant for short chain electroactive thiols.

Summary

The presence of a redox center on the surface of a self-assembled monolayer provides a sensitive and useful probe for monolayer structure. The pyRu$(NH_3)_5^{2+/3+}$ redox centers in the self-assembled monolayers exhibit ideal behavior under reversible CV conditions. The average environment around the redox centers is uniform across the monolayer. The formal potential is consistent with the redox centers residing in the aqueous phase outside of the alkane portion of the monolayer.

Measurement of electron-transfer kinetics by cyclic voltammetry and chronoamperometry yields information about monolayer structure which is not apparent under reversible conditions. Chronoamperometry and Tafel plots are the preferred methods for kinetic measurements. A nearly uniform rate of electron transfer is observed for the redox centers in a monolayer, which implies that factors affecting the rate (distance, conformation of the alkyl chain) do not vary significantly within the monolayer. Many of the monolayers in this study exhibit evidence for a population of fast redox centers which can affect the apparent rate of electron transfer at low overpotentials. The fast centers may be electroactive thiols in loosely packed domains (defects) so that chain motion provides a mechanism for rapid electron transfer.

The standard rate constant for the electroactive monolayer is primarily determined by the number of methylenes in the tether connecting the redox center to the electrode. In mixed monolayers, the nature of the terminal group (COOH or CH_3) in the diluent thiol has no significant effect on the standard rate constant. Coassembly of the electroactive thiol with the diluent thiol in the HS–C_{15}–Ru monolayers decreases the standard rate constant by a factor of ca. 3. Diluent thiols either inhibit chain motion of the electroactive thiols or hold the redox center further away from the electrode surface. The slopes of the Tafel plots are symmetrical and consistent with predictions of Marcus theory. The solvent reorganization parameter of the redox centers is smaller than anticipated on the basis of Marcus theory. Values of λ decrease as the chain length to the redox centers becomes shorter. A small difference in the standard rate constant for the anodic and the cathodic branches of the Tafel plots implies that the conformation of the monolayer is dependent on either the oxidation state of the redox centers or the electrode potential. The standard rate constants from the Tafel plots obey the exponential tunneling equation, with the tunneling parameter β being 1.06 ± 0.04 per CH_2. The predictions of through-space electron tunneling are not confirmed both in the slopes of the Tafel plots and in the value of the tunneling constant. Electron tunneling through the alkyl chain is proposed as the electron-transfer mechanism.

Appendix. Electron-Transfer Theory for an Electroactive Monolayer

A theory of through-space electron tunneling[29] to attached redox centers on an electrode should include factors such as (a) the density of electron donor and electron acceptor states associated with the redox centers, (b) the density of occupied and empty states in the metal, and (c) the height, shape, and thickness of the energy barrier that separates the redox centers and the electrode. The rate constant for the reduction of an oxidized center can be calculated by

$$k_{app} = k \int \rho(E)\, n(E)\, D_{OX}(E)\, P(E)\, dE \quad (4)$$

The integration is performed over a range of energies about the Fermi energy of the metal; the zero point is defined by the Fermi energy. $\rho(E)$ is the density of states in the metal and is assumed to be constant over the range of energies necessary for accurate integration. $n(E)$ is the Fermi distribution function for occupied states in the metal:

$$n(E) = 1/\{1 + \exp(E/kT)\} \quad (5)$$

$P(E)$ is the probability of tunneling through the energy barrier. For the case of direct elastic tunneling through a trapezoidal energy barrier, an approximate expression for $P(E)$ is given by[31]

$$P(E) = (E_B - E + e\eta/2) \exp(-\beta d) \quad (6)$$

$$\beta = (2(2m)^{1/2}/\hbar)(E_B - E + e\eta/2)^{1/2} \quad (7)$$

β is the tunneling constant, E_B is the average barrier height at zero overpotential, m is the mass of the electron, e is the charge of the electron, and d is the thickness of the barrier. Equation 7 assumes that all of the potential drop occurs across the barrier, so that changes in the average barrier height are proportional to $\eta/2$. The average barrier height increases as overpotential becomes more positive. Finally, $D_{OX}(E)$ is the density of acceptor states as defined in Marcus theory.[44]

$$D_{OX}(E) = \Gamma_{OX}(4\pi\lambda kT)^{-1/2} \exp\{-(E - \lambda - e\eta)^2/(4\lambda kT)\} \quad (8)$$

Γ_{OX} is the coverage in mol/cm^2, and λ is the solvent reorganization parameter. Numerical integration of eq 4 provides k_{app} as a function of distance, overpotential, average barrier height, and solvent reorganization parameter. The equivalent apparent rate constant for oxidation of a reduced center is obtained by replacing D_{OX} with D_{RED} (λ's are assumed to be the same for the OX and RED species) and the Fermi distribution function with its complement $(1 - n(E))$. Equation 4 contains an unknown constant factor. In the Tafel plots, all apparent rate constants obtained from eq 4 are scaled relative to k°_{app}, which in turn is obtained by doing the integration at $\eta = 0$.

Figure 2 was calculated with $\lambda = 0.6$ eV (based on the experimental Tafel plots) and with $E_B = 2.4$ eV. An appropriate value for E_B is estimated as follows. Calculations of k_{app} as a function of d using eq 4 confirm that k_{app} decays exponentially with distance (eq 2). At $\eta = 0$, the tunneling constant β is essentially identical with the value predicted by classical tunneling theory:

$$\beta = (1.025/(\text{Å eV}^{1/2}))(E_B)^{1/2} \quad (9)$$

Equation 9 assumes that m is the mass of the electron in vacuum. Experimental values of β are close to 1.5 $Å^{-1}$ for metal/monolayer/metal tunneling junctions,[2,3] where the monolayer is a fatty acid deposited by either the Langmuir–Blodgett or the self-assembly method. Solving eq 9 for E_B yields a value of 2.1 eV. Simmons[31] noted that image forces result in an effective barrier height which is smaller than the true barrier height. The true barrier height for the Al/Al_2O_3/monolayer/Al tunneling junction is calculated to be between 1.9 and 2.8 eV.[3] To correct this value to the Au/monolayer/redox center system, we note that the work function of aluminum is estimated to be 4.2 eV[3] and that the work function of a metal at 0 V vs SCE (the formal potential of the redox center) is estimated to be 4.7 eV.[32] Hence, the true barrier height should lie between 2.4 and 3.3 eV for the Ru$(NH_3)_5$py redox center attached by an alkane chain to the gold electrode. Image forces, which are difficult to estimate, are expected to reduce the true barrier height to a value between 1.5 and 3.0 eV. Predicted β's then range from 1.3 to 1.8 $Å^{-1}$.

To calculate theoretical Tafel plots without through-space tunneling, $P(E)$ is set to a constant value and eq 4 is integrated.

Supplementary Material Available: Text describing a chronoamperometry simulation for a monolayer with varying degrees of disorder and figures of a CA simulation, CA plots for selected mixed monolayers, and Tafel plots for all of the mixed monolayers listed in Table I (19 pages). Ordering information is given on any current masthead page.